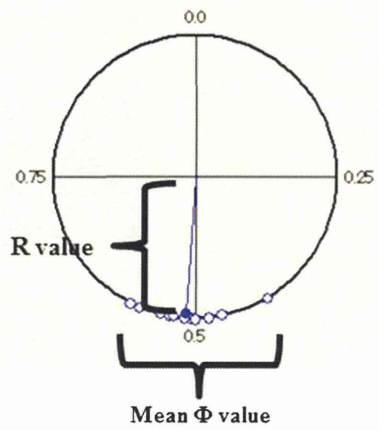

Fig. 4 Circular phase. The touch-down phases of both hindlimbs were quantitatively assessed within one cycle as the time taken from when the right hindlimb lifted-off till the time it touched-down again. During this, the touch-down timing of the left hindlimb was plotted on a pie chart, which provided two indicators: the R and mean Φ values. The mean Φ value was normalized to 50 %. Some dispersion was shown in the R values, with dispersion decreasing as the R value approached 1 and increasing as the R value approached 0. That is, when the mean Φ value was normalized to 0.5, the R value approached 1

Statistical analysis

To analyze BBB scores, the Welch test was performed with the independent variables between the groups. To analyze 3D kinematics data during walking at day 14 post-injury, the Welch test was used to compare the phase values of gait cycles and SYM-E values for the ankle joint ROM between the groups. In this study, a p value of <0.05 was considered statistically significant.

Results

Ankle-joint angle movement during NMES

Figure 5 shows the average ankle joint ROM immediately after stimulation and at 5, 10, and 15 min post-stimulation. During the first 10 cycles of stimulation, the average observed ankle ROM of the iSCI-NMES 75-Hz group was 39°. After 5 min of NMES, the range decayed to 18 degrees, representing a significant decrease (Fig. 5a). The average observed ankle ROM of the iSCI-NMES 8-kHz group was 16 degrees. After 5 min of NMES, the range decayed to 6°, representing a significant decrease. The average ankle ROM of both groups remained greater than zero until the completion of the NMES session; however, significant decay continued at 10 and 15 min post-stimulation (Fig. 5b).

Over-ground walking locomotor score

The mean BBB scores of the iSCI-NT group were as follows: 1 day post-injury, 0 ± 0; 3 days post-injury, 0.8 ± 0.4; 7 days post-injury, 5.0 ± 1.2; 10 days post-injury, 11.6 ± 2.3; and 14 days post-injury, 14.4 ± 1.0. The mean BBB scores of the iSCI-NMES 75-Hz group were as follows: 1 day post-injury, 0 ± 0; 3 days post-injury, 1.4 ± 0.5; 7 days post-injury, 6.2 ± 1.2; 10 days post-injury, 10.4 ± 2.3; and 14 days post-injury, 14.8 ± 0.7. Moreover, the mean BBB scores of the iSCI-NMES 8-kHz group were as follows: 1 day post-injury, 0 ± 0; 3 days post-injury, 1.4 ± 0.5; 7 days post-injury, 6.2 ± 1.2; 10 days

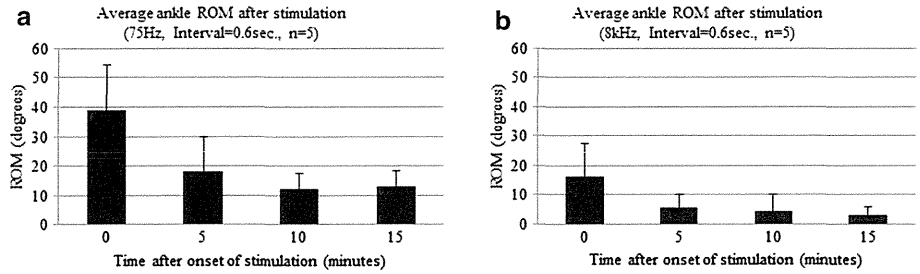

Fig. 5 Changes in mean leg range of motion over time. The changes in mean limb joint range of motion (ROM) immediately after the start of stimulation and at 5, 10, and 15 min later. **a** In the 75-Hz stimulation frequency group, good ROM is observed immediately after the start of stimulation; however, a significant decrease in ROM is observed 5 min later ($p = 0.001$). **b** In the 8-kHz stimulation frequency group, joint ROM is lower than that of the 75-Hz group immediately after stimulation, and then significantly decreases after 5 min

post-injury, 10.4 ± 2.3; and 14 days post-injury, 14.8 ± 0.7. There were no significant differences in BBB scores between the groups (Fig. 6).

Recovery of locomotor coordination in 3D kinematic analysis

Phase relationships in the gait cycle (Fig. 7)

In the Normal-CT group, the stance phase value was 80.8 ± 2.9 %, the swing phase value was 19.2 ± 2.9 %, and the double support phase value was 30.4 ± 9.4 % at 13.7 cm/s. Stride length value was 9.3 ± 4.4 cm. For the iSCI-NT group, the stance phase value was 73.8 ± 7.8 %, the swing phase value was 26.2 ± 7.8, and the double support phase value was 20.8 ± 16.9 %. The stride width value was 10.4 ± 4.8 cm. For the iSCI-NMES 75-Hz group, the stance phase value was 73.4 ± 6.2 %, the swing phase value was 26.6 ± 6.2 %, the double support phase value was 16.0 ± 10.8 %, and the stride length value was 11.7 ± 1.8 cm. For the iSCI-NMES 8-kHz group, the stance phase value was 76.9 ± 5.3 %, the swing phase value was 23.1 ± 5.3 %, the double support phase value was 35.8 ± 12.0 %, and the stride length value was 11.6 ± 1.5 cm. The injury group (iSCI-NT), treatment groups (iSCI-NMES 75 Hz and 8 kHz), and normal group (Normal-CT) showed no significant difference in the ratio of the two phases for stance and swing

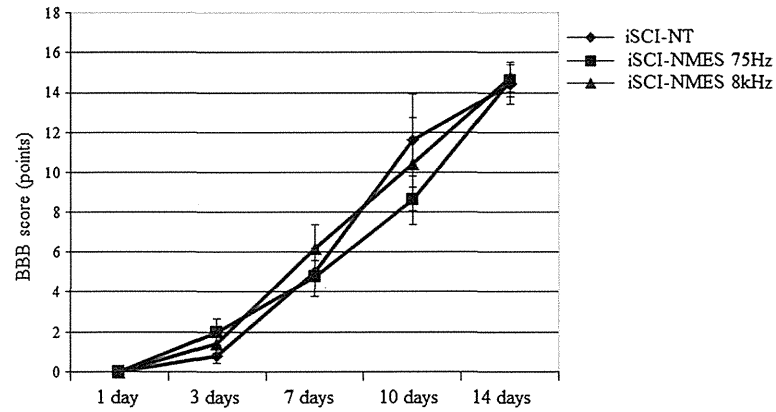

Fig. 6 BBB score. There is no significant difference in *BBB scores* observed between either experimental group at any time

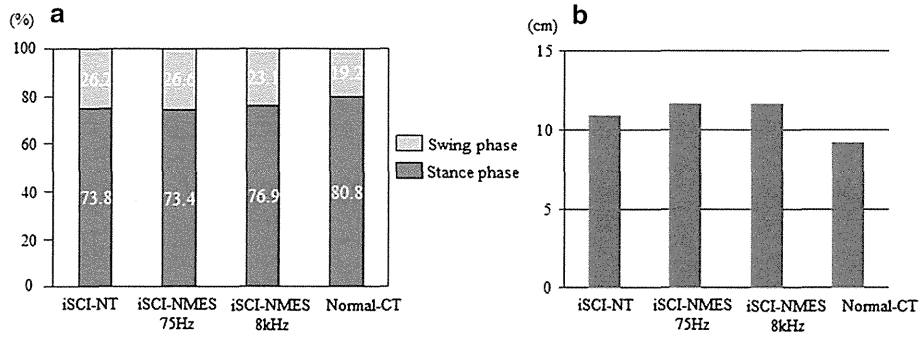

Fig. 7 Phase relationships in gait cycle. These graphs show the two phases for stance and swing (**a**), stride length (**b**). There were no significant differences between the iSCI-NMES and iSCI-NT groups

(Fig. 7a). Furthermore, compared with the normal group, the injury group and treatment group tend to exhibit longer stride length (Fig. 7b); however, there is no significant difference observed for either.

Foot trajectories and normalized joint angles

The graph marking the sagittal trajectory of the leg markers shows that in the normal group, the leg moves linearly vertical during the stance phase, then swings up vertically in an arc, and swings forward (Fig. 8a). In the spinal injury control group, the vertical movement during the stance phase was not linear (Fig. 8b); however, in the NMES treatment group, all movements were linear and an improvement was observed (Fig. 8c, d). On the other hand, during the swing phase, compared with the normal group, none of the experimental groups exhibited vertical arc-like movement; there was no improvement in horizontal leg movement during the swing phase (Fig. 8).

In the normalized joint angle trajectory graph, ROM greatly changed during the swing phase in the treatment group (Fig. 9), whereas in the coronal plane of the joint ROM trajectory, particularly in the iSCI-NMES 8-kHz group, the pattern during the swing phase approached normal, and an improvement in ankle eversion was observed (Fig. 10).

Circular phase (Fig. 11)

For normal rats, the mean Φ value was 0.49 ± 0.06 % and the R value was 0.87 ± 0.05. For the iSCI-NT group, the mean Φ value was 0.5 ± 0.05 and the R value was 0.59 ± 0.12. For the iSCI-NMES 75-Hz group, the mean Φ value was 0.6 ± 0.01 and the R value was 0.73 ± 0.09 (Fig. 11). For the iSCI-NMES 8-kHz group, the mean Φ value was 0.4 ± 0.08 and the R value was 0.87 ± 0.03 (Fig. 11). No significant differences were observed in the mean Φ values between the four groups. The iSCI-NT and iSCI-NMES 75-Hz groups had significantly smaller R values than the Normal-CT group; however, the iSCI-NMES 75-Hz group exhibited greater improvement than the iSCI-NT group ($p = 0.06$; Fig. 11). The iSCI-NMES 8-kHz group had significantly smaller R values than the iSCI-NT group ($p < 0.01$; Fig. 11).

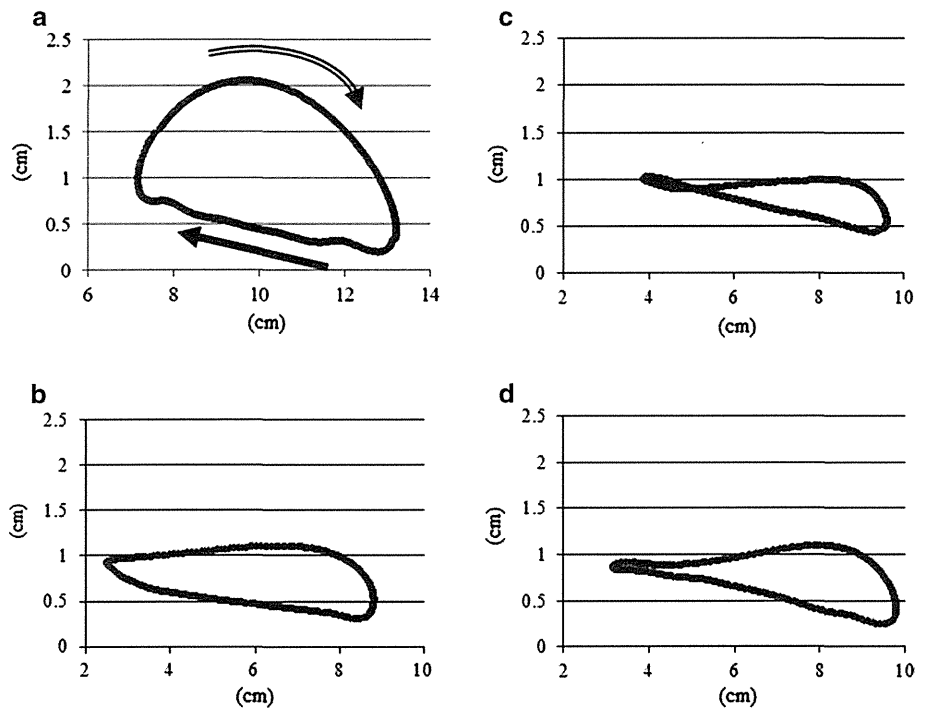

Fig. 8 Foot trajectories. This graph shows the sagittal trajectory of the leg markers. In the normal group, the leg moves *linearly vertically* during the stance phase (*filled right arrow*); then, during the swing phase (*right double arrow*), swings up *vertically* in an arc and swings forward (**a**). In the spinal injury control group, the *vertical* movement during the stance phase is not linear (**b**); however, in the NMES treatment group, all movements are linear and an improvement is observed (**c** 75 Hz, **d** 8 kHz). On the other hand, during the swing phase, compared with the normal group, no groups exhibited *vertical arc-like* movements and there was no improvement in *horizontal* leg movement during the swing phase

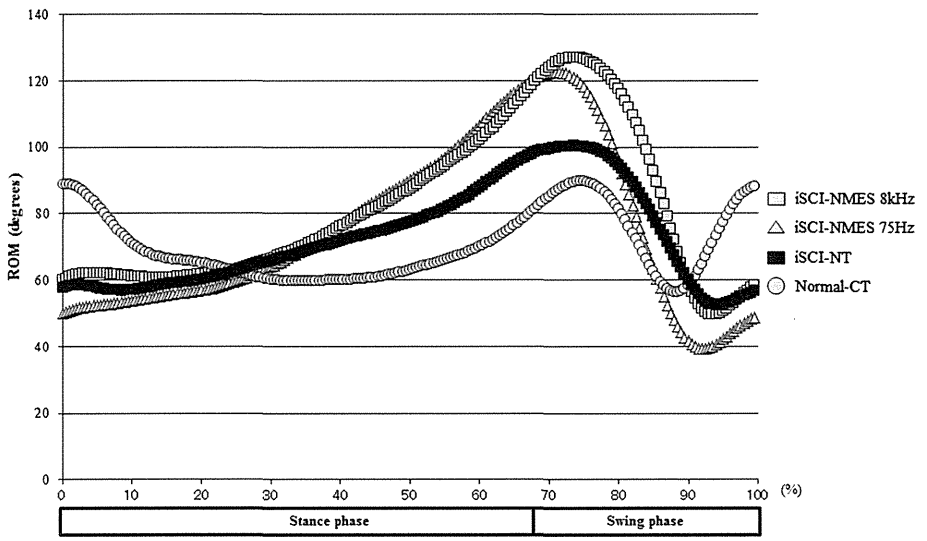

Fig. 9 Normalized joint angles (three-directional mean graph). This graph shows the normalized range of motion trajectory for joints. Although joint angle range of motion changes during the swing phase in the treatment group, the change is not great compared with the injury control group

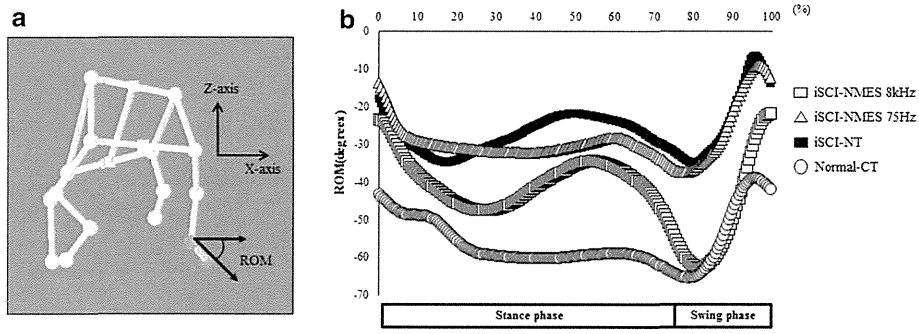

Fig. 10 Normalized joint angles (mean graph of the coronal plane). This graph shows the joint range of motion trajectory in the coronal plane to assess ankle eversion (**a**), which becomes close to the pattern of the normal group in the 8-kHz group (iSCI-NMES 8 kHz), particularly during the swing phase (**b**), and an improvement in eversion is observed

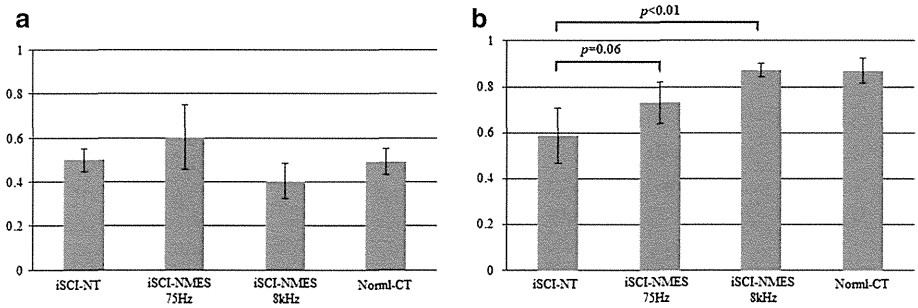

Fig. 11 Mean Φ and R values in circular phase. The circular phase quantifies the touchdown phase of both hindlimbs. Upon comparing the circular phase of each group, there is no significant difference observed in mean Φ value (**a**); however, when comparing the experimental groups with the injury control group, the R value tends to improve in the iSCI-NMES 75-Hz group ($p = 0.06$), and a significant difference is observed in the iSCI-NMES 8-kHz group ($p < 0.01$) (**b**)

Angle–angle plots

An angle–angle plot graph of the left and right ankles determined by 3D kinematic gait analysis revealed that when walking at the speed of 13.7 cm/s, the symmetry index was 7.6 ± 2.0 in the Normal-CT group, 18.0 ± 7.9 in the NT group, 17.7 ± 9.0 in the iSCI-NMES 75-Hz group, and 15.4 ± 7.4 in the iSCI-NMES 8-kHz group. Although improvements were insufficient, a marginal improvement was observed in the iSCI-NMES 8-kHz group (Fig. 12).

Discussion

Central pattern generators (CPG) in brainstem–spinal cord neural networks associated with gait, producing rhythmic movements. These stimulate peripheral sensory input from muscular spindles and the golgi tendon organ, which contribute to the mechanism in which NMES improves motor function, and this repetitive peripheral sensory input is required for neural plasticity [23, 24]. Jung et al. reported that in a NMES rat model using embedded electrodes, the stimulation of gait rhythm after incomplete spinal cord injury significantly improved motor function of the hindlimbs in the short term [18]. In a previous rat NMES model using needle electrodes, we successfully created a

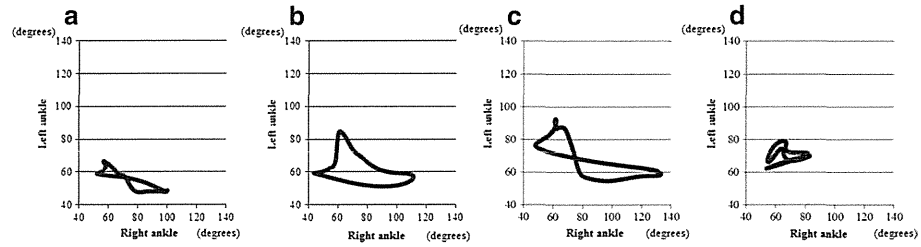

Fig. 12 Angle–angle plots. This graph shows the angle–angle plots of the joints in each group. The symmetry index is 18.0 ± 7.9 in the Normal-CT group (**a**), 17.7 ± 9.0 in the iSCI-NMES 75-Hz group (**b**), 15.4 ± 7.4 in the iSCI-NMES 8-kHz group (**c**), and 7.6 ± 2.0 in the Normal-CT group (**d**). Although a marginal improvement is observed in the iSCI-NMES 8-kHz group, no significant improvement is achieved

less-invasive NMES therapy model [21]. On the other hand, we were unable to find any reports examining conditions under which the stimulation of gait rhythm using NMES effectively improved motor function.

When stimulating gait rhythm using NMES, muscle fatigue can be a problem. In the report by Jung et al. describing embedded electrodes used in the agonist muscles of the hip, a significant decrease in ROM was observed less than 1 week after the start of stimulation [18]. In a previous NMES model that used needle electrodes in normal rats, gait rhythm was successfully stimulated under sedation; however, a significant decrease in ROM was observed less than 5 min after the start of stimulation [17]. This was attributed to fatigue of the stimulated muscle because of open-loop stimulation. To address this reduced ROM due to muscle fatigue, stimulation with a higher instead of a lower frequency is an effective method to increase the electrical stimulation current threshold and impede muscle fatigue [25]. Furthermore, Ward et al. reported that stimulation with alternating currents in kHz frequency is effective for muscle fatigue in NMES [26, 27]. We previously reported that when stimulating gait rhythm, stimulation with alternating currents in kHz frequency could possibly be used for motor therapy [17]. In the present study, ROM was significantly smaller in the 8-kHz group than in the 75-Hz group, and the effect on muscle fatigue was not fully examined. As previously reported, this is believed to be because the stimulation intensity was set at three times the threshold known to produce a visually observable twitch. However, to maintain the conditions other than the stimulation frequency in the present study, the stimulation intensity was 1.5 times the threshold intensity that produces a visually observable twitch. In a similar model using embedded electrodes in the agonist muscles of the hip, Jung et al. reported that by day 14 post-injury, NMES treatment given 15 min/day for 5 days, starting 1 week after injury, resulted in a significant improvement in the touchdown phase of both hindlimbs, as well as in the coordination of the left and right hips [18]. In the present study, we observed an improvement in the touchdown phase of both hindlimbs in the iSCI-NMES 75-Hz group, as well as a significant improvement in the iSCI-NMES 8-kHz group (Fig. 11). Although the interlimb coordination of both hindlimbs tended to improve, there was no significant improvement observed. Therefore, in Jung et al.'s model [18], since the treatment was given for 5 days and embedded electrodes were used, stimulation of gait rhythm via actual stimulation of motor points during the 15-min stimulation period may have been enabled. However, in a study with identical

conditions other than the stimulation frequency, motor function improved more in the iSCI-NMES 8-kHz group than in the iSCI-NMES 75-Hz group. This result supports the notion that kHz stimulation is effective in the stimulation of gait rhythm to treat spinal injury-induced motor paralysis.

Although the mechanism in which stimulation with alternating currents in kHz frequency effectively improves motor function is not understood in detail, as reported by Ward et al., stimulation with alternating currents in kHz frequency effectively stimulates fatigue-resistant fibers and may produce greater sensory-feedback with the central pattern generator [27].

Limitations of the present study were that at 3 days, the stimulation treatment period was short and that evaluations were only conducted for 2 weeks. In future, there should be a longer period of study. Furthermore, a stimulation frequency of 8 kHz has not been shown to be clinically effective; therefore, examinations should be performed under conditions that enable the clinical application of kHz frequency stimulation. In future, we plan to examine stimulation conditions that effectively improve motor function, as well as the effect of combination therapy with various regenerative therapies to help establish effective rehabilitation during the acute phase after spinal cord injury and regenerative therapy.

Conclusions

We employed a less-invasive NMES therapy model with needle electrodes to examine the effectiveness of high-frequency stimulation for gait rhythm. Three-dimensional gait analysis revealed improved toe clearance and touchdown phase of both hindlimbs in the NMES group, with a particularly significant improvement in the 8-kHz group. This suggests that stimulation with alternating currents in the kHz frequency is effective in gait rhythm stimulation by NMES.

Authors' contributions

TK was responsible for data collection, data analysis, experimental design, and took the lead on manuscript writing and figure design. SH, IY, YY, MA, SY, NN, and TY contributed to data collection and data analysis. TT contributed to manuscript preparation. All authors read and approved the final manuscript.

Acknowledgements

This work was supported in part by JSPS KAKENHI (24592199).

Competing interests

The authors declare that they have no competing interests.

Received: 7 July 2015 Accepted: 15 October 2015
Published online: 29 October 2015

References

1. Ramer LM, Ramer MS, Steeves JD. Setting the stage for functional repair of spinal cord injuries: a cast of thousands. Spinal Cord. 2005;43:134–61.
2. Barbeau H, McCrea DA, Odonovan MJ, Rossignol S, Grill WM, Lemay MA. Tapping into spinal circuits to restore motor function. Brain Res Brain Res Rev. 1999;30:27–51.
3. Field-Fote EC. Combined use of body weight support, functional electric stimulation, and treadmill training to improve walking ability in individuals with chronic incomplete spinal cord injury. Arch Phys Med Rehabil. 2001;82:818–24.
4. Wirz M, Zemon DH, Rupp R, Scheel A, Colombo G, Dietz V, et al. Effectiveness of automated locomotor training in patients with chronic incomplete spinal cord injury: a multicenter trial. Arch Phys Med Rehabil. 2005;86:672–80.
5. Nudo RJ, Milliken GW, Jenkins WM, Merzenich MM. Use-dependent alterations of movement representations in primary motor cortex of adult squirrel monkeys. J Neurosci. 1996;16:785–807.

6. Nudo RJ, Milliken GW. Reorganization of movement representations in primary motor cortex following focal ischemic infarcts in adult squirrel monkeys. J Neurophysiol. 1996;75:2144–9.
7. Francis S, Lin X, Aboushoushah S, White TP, Phillips M, Bowtell R, et al. fMRI analysis of active, passive and electrically stimulated ankle dorsiflexion. NeuroImage. 2009;44:469–79.
8. Liepert J, Bauder H, Wolfgang HR, Miltner WH, Taub E, Weiller C. Treatment-induced cortical reorganization after stroke in humans. Stroke. 2000;31:1210–6.
9. Beekhuizen KS, Field-Fote EC. Massed practice versus massed practice with stimulation: effects on upper extremity function and cortical plasticity in individuals with incomplete cervical spinal cord injury. Neurorehabil Neural Repair. 2005;19:33–45.
10. Field-Fote EC, Tepavac D. Improved intralimb coordination in people with incomplete spinal cord injury following training with body weight support and electrical stimulation. Phys Ther. 2002;82:707–15.
11. Popovic MR, Thrasher TA, Adams ME, Takes V, Zivanovic V, Tonack MI. Functional electrical therapy: retraining grasping in spinal cord injury. Spinal Cord. 2006;44:143–51.
12. Bouyer LJ. Animal models for studying potential training strategies in persons with spinal cord injury. J Neurol Phys Ther. 2005;29:117–25.
13. Edgerton VR, Roy RR. Robotic training and spinal cord plasticity. Brain Res Bull. 2009;78:4–12.
14. Courtine G, Gerasimenko Y, van den Brand R, Yew A, Musienko P, Zhong H, et al. Transformation of non-functional spinal circuits into functional states after the loss of brain input. Nat Neurosci. 2009;12:1333–42.
15. Ichihara K, Venkatasubramanian G, Abbas JJ, Jung R. Neuromuscular electrical stimulation of the hindlimb muscles for movement therapy in a rodent model. J Neurosci Methods. 2009;176:213–24.
16. Jung R, Ichihara K, Venkatasubramanian G, Abbas JJ. Chronic neuromuscular electrical stimulation of paralyzed hindlimbs in a rodent model. J Neurosci Methods. 2009;183:241–54.
17. Kanchiku T, Lynskey JV, Protas D, Abbas JJ, Jung R. Neuromuscular electrical stimulation induced forelimb movement in a rodent model. J Neurosci Methods. 2008;167:317–26.
18. Jung R, Belanger A, Kanchiku T, Fairchild M, Abbas JJ. Neuromuscular stimulation therapy after incomplete spinal cord injury promotes recovery of interlimb coordination during locomotion. J Neural Eng. 2009;6:055010.
19. Szecsi J, Fornusek C, Krause P, Straube A. Low-frequency rectangular pulse is superior to middle frequency alternating current stimulation in cycling of people with spinal cord injury. Arch Phys Med Rehabil. 2007;88:338–45.
20. Szecsi J, Schiller M. FES-propelled cycling of SCI subjects with highly spastic leg musculature. NeuroRehabilitation. 2009;24:243–53.
21. Kanchiku T, Kato Y, Suzuki H, Imajo Y, Yoshida Y, Moriya A, et al. Development of less invasive neuromuscular electrical stimulation model for motor therapy in rodents. J Spinal Cord Med. 2012;35:162–9.
22. Thota AK, Watson SC, Knapp E, Thompson B, Jung R. Neuromechanical control of locomotion in the rat. J Neurotrauma. 2005;22:442–65.
23. Khaslavskaia S, Ladouceur M, Sinkjaer T. Increase in tibialis anterior motor cortex excitability following repetitive electrical stimulation of the common peroneal nerve. Exp Brain Res. 2002;145:309–15.
24. Perez MA, Field-Fote EC, Floeter MK. Patterned sensory stimulation induces plasticity in reciprocal IA inhibition in humans. J Neurosci. 2003;23:2014–8.
25. Matsunaga T, Shimada Y, Sato K. Muscle fatigue from intermittent stimulation with low and high frequency electrical pulses. Arch Phys Med Rehabil. 1999;80:48–53.
26. Ward AR. Electrical stimulation using kilohertz frequency alternating current. Phys Ther. 2009;89:181–90.
27. Ward AR, Robertson VJ. The variation in fatigue rate with frequency using kHz frequency alternating current. Med Eng Phys. 2000;22:637–46.

Koda et al. BMC Res Notes (2015) 8:545
DOI 10.1186/s13104-015-1430-3

BMC Research Notes

CASE REPORT Open Access

Resolution of low back symptoms after corrective surgery for dropped-head syndrome: a report of two cases

Masao Koda[1*], Takeo Furuya[1], Taigo Inada[1], Koshiro Kamiya[1], Mitsutoshi Ota[1], Satoshi Maki[1], Osamu Ikeda[1], Masaaki Aramomi[1], Kazuhisa Takahashi[1], Masashi Yamazaki[2] and Chikato Mannoji[3]

Abstract

Background: Cervical deformity can influence global sagittal balance. We report two cases of severe low back pain and lower extremity radicular pain associated with dropped-head syndrome. Symptoms were relieved by cervical corrective surgery.

Case presentation: Two Japanese women with dropped head syndrome complained of severe low back pain and lower extremity radicular pain on walking. Radiographs showed marked cervical spine kyphosis and lumbar spine hyperlordosis. After cervicothoracic posterior corrective fusion was performed, cervical kyphosis was corrected and lumbar lordosis decreased, and low back pain and leg pain were relieved in both patients.

Conclusions: Cervical deformity can influence global sagittal balance. Marked cervical kyphosis in patients with dropped-head syndrome can induce compensatory thoracolumbar hyperlordosis. Low back symptoms in patients with dropped-head syndrome are attributable to this compensatory lumbar hyperlordosis. Symptoms of lumbar canal stenosis may result from cervical deformity and can be improved with cervical corrective surgery.

Keywords: Dropped-head syndrome, Sagittal imbalance, Corrective surgery, Lumbar canal stenosis

Background

Dropped-head syndrome is defined as apparent weakness of the neck extensor muscles that results in difficulty lifting the head against gravity and consequent impairment of activities of daily living. Its main symptoms include impaired forward vision, neck pain, and myelopathy and/or radiculopathy [1, 2].

We report two cases of severe low back pain and lower extremity radicular pain concomitant with dropped-head syndrome. The patients' symptoms were relieved after cervical corrective surgery. The present manuscript confirmed to CARE checklist (Additional file 1).

Case presentation

Case 1

A 72-year-old Japanese woman complained of hand numbness and gait disturbance because of cervical spondylotic myelopathy. The patient underwent 3rd cervical vertebra (C3) to 6th cervical vertebra (C6) laminoplasty (Fig. 1). Her postoperative course was uneventful. Two months after the surgery, she complained of an inability to lift her head because of neck extensor muscle weakness. The patient gradually developed hand numbness. Magnetic resonance imaging (MRI) revealed spinal cord compression both anteriorly and posteriorly at the C4–5 and C5–6 levels. A whole-spine radiograph showed marked kyphosis at the cervical spine and hyperlordosis at the lumbar spine. The angle between C2 and C7 was −35.8°, the 1st thoracic vertebra (T1) slope was 18°, and lumbar lordosis was 43.8° (Fig. 1). The patient complained

*Correspondence: masaokod@gmail.com
[1] Department of Orthopedic Surgery, Chiba University Graduate School of Medicine, 1-8-1 Inohana, Chuo-Ku, Chiba 260-8670, Japan
Full list of author information is available at the end of the article

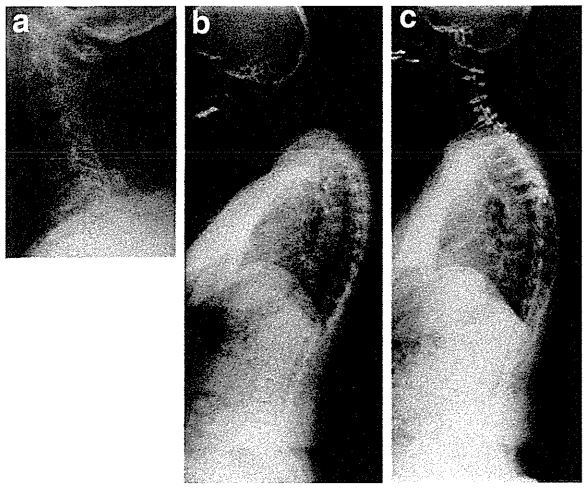

Fig. 1 Case 1 radiographs. **a** Lateral plain radiograph of the cervical spine after laminoplasty for cervical spondylotic myelopathy showing normal sagittal alignment. The patient complained of head drop and severe low back and lower extremity pain 2 months after laminoplasty. **b** Lateral whole-spine radiograph showing marked cervical spine kyphosis and lumbar spine hyperlordosis. **c** After cervical corrective fusion (C2–C4), cervical kyphosis and lumbar hyperlordosis, as well as lumbar spine symptoms, were relieved. *C* cervical vertebra

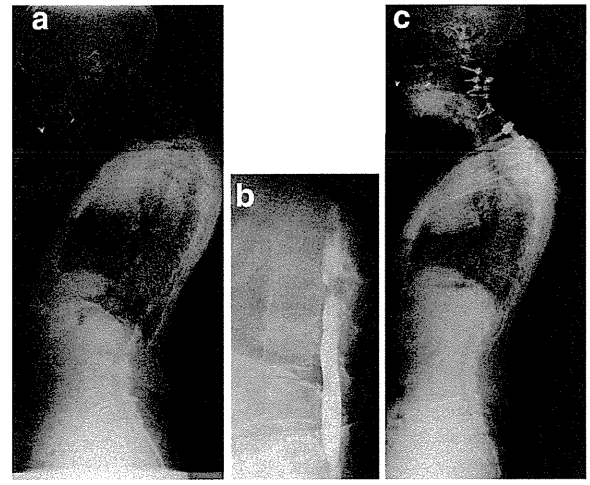

Fig. 2 Case 2 pre- and postoperative radiographs. The patient complained of head drop and severe low back and lower extremity pain preoperatively. **a** Lateral whole-spine radiograph showing marked cervical spine kyphosis and lumbar spine hyperlordosis. **b** Preoperative myelogram of lumbar spine showing marked canal stenosis between L2 and L3. **c** Cervical kyphosis and lumbar hyperlordosis were corrected, and low back pain and lower extremity pain were relieved, after cervical corrective fusion (C2–C6). *C* cervical vertebra, *L* lumbar vertebra

of difficulty with horizontal gaze, hand numbness, and low back and bilateral leg pain after walking for 10 min.

The patient underwent laminectomy from C3 to C6 and posterior corrective fusion from C2 to T4, which corrected the cervical kyphosis. Postoperatively, the angle between C2 and C7 improved to 17.7°, T1 slope was 16.5°, lumbar lordosis decreased from 43.8° to 31.4°, and the patient experienced relief of her low back pain and bilateral leg pain.

Case 2

A 64-year-old Japanese woman complained of weakness of her left hand, dropped head, and right thigh pain after walking 10 meter. Magnetic resonance imaging revealed anterior and posterior spinal cord compression at the C4–5 and C5–6 levels. A whole-spine radiograph showed marked kyphosis at the cervical spine and hyperlordosis at the lumbar spine. The C2 to C7 ngle was −50°, T1 slope was 17°, and lumbar lordosis was 50° (Fig. 2). Myelography revealed marked lumbar canal stenosis at the L2–3 level. The patient underwent laminectomy from C3 to C6 followed by C4–5 and C5–6 anterior cervical diskectomy and fusion as well as posterior corrective fusion from C2 to T6. Cervical kyphosis was corrected, and the angle between C2 and C7 improved to 22.2°. Postoperative T1 slope was 25°, an increase of 8° from preoperatively. Lumbar lordosis decreased from 50° to 25°. Low back pain and right thigh pain were relieved.

Discussion

Deformity of the thoracolumbar spine can induce cervical deformity [3]. Smith et al. reported that patients with positive sagittal malalignment tend to compensate with cervical hyperlordosis to maintain horizontal gaze, and that surgical correction of thoracolumbar sagittal malalignment results in resolution of cervical hyperlordosis via reciprocal change. This spontaneous correction of cervical deformity after correction of global sagittal balance by lumbar pedicle subtraction osteotomy has been reported [4].

Conversely, cervical deformity can influence global sagittal balance. The marked cervical kyphosis observed in patients with dropped-head syndrome can induce compensatory thoracolumbar hyperlordosis. The patient in case 2 showed a postoperative increase in T1 slope, suggesting a compensatory extension of the thoracolumbar spine. Low back pain in patients with dropped-head syndrome is attributed to this compensatory mechanism. Extension of the lumbar spine can induce buckling of the yellow ligament and possibly resulting in exacerbation of lumbar canal stenosis and worsening associated symptoms [5]. Therefore, patients with marked cervical kyphosis with compensatory lumbar hyperlordosis experience worsening symptoms of lumbar canal stenosis. If the hyperlordosis and hyperlordosis-related aggravation of lumbar canal stenosis symptoms are actually secondary

to cervical kyphosis, low back symptoms can be resolved by correction of cervical kyphosis. In the present cases, compensatory lumbar hyperlordosis was mitigated by correction of cervical kyphosis.

Conclusion

Lumbar canal stenosis symptoms can result from cervical deformity and can be improved by cervical corrective surgery.

Consent

Written informed consent was obtained from both patients for publication of this Case Report and any accompanying images. A copy of the written consent is available for review by the Editor-in-Chief of this journal.

Additional files

Additional file 1: CARE checklist for case reports. The present manuscript confirmed to CARE checklist.

Authors' contributions

MK, TF, TI, KK, MO, and SM carried out the treatment and follow-up of the patients. OI obtained and assessed images of the patients. MA, KT, MY, and CM conceived of the study, participated in its design and coordination, and helped to draft the manuscript. All authors read and approved the final manuscript.

Author details

[1] Department of Orthopedic Surgery, Chiba University Graduate School of Medicine, 1-8-1 Inohana, Chuo-Ku, Chiba 260-8670, Japan. [2] Department of Orthopedic Surgery, University of Tsukuba, 1-1-1 Tennodai, Tsukuba 30585775, Japan. [3] Department of Orthopedic Surgery, Chiba Aoba Municipal Hospital, 1273-2 Aoba-cho, Chuo-Ku, Chiba 2600852, Japan.

Acknowledgements

There is no source of funding for all authors.

Competing interests

The authors declare that they have no competing interests.

Received: 19 March 2015 Accepted: 9 September 2015
Published online: 07 October 2015

References

1. Sharan AD, Kaye D, Charles Malveaux WM, Riew KD. Dropped head syndrome: etiology and management. J Am Acad Orthop Surg. 2012;20:766–74.
2. Nakanishi K, Taneda M, Sumii T, Yabuuchi T, Iwakura N. Cervical myelopathy caused by dropped head syndrome. Case report and review of the literature. J Neurosurg Spine. 2007; 6:165–8.
3. Smith JS, Lafage V, Schwab FJ, Shaffrey CI, Protopsaltis T, Klineberg E, et al. Prevalence and type of cervical deformity among 470 adults with thoracolumbar deformity. Spine. 2014;17:1001–9.
4. Smith JS, Shaffrey CI, Lafage V, Blondel B, Schwab F, Hostin R, et al. Spontaneous improvement of cervical alignment after correction of global sagittal balance following pedicle subtraction osteotomy. J Neurosurg. 2012;17:300–7.
5. Truumees E. Spinal stenosis: pathophysiology, clinical and radiologic classification. Instr Course Lect. 2005;54:287–302.

Eur Spine J
DOI 10.1007/s00586-015-3888-z

ORIGINAL ARTICLE

Bone union and remodelling of the non-ossified segment in thoracic ossification of the posterior longitudinal ligament after posterior decompression and fusion surgery

Masao Koda[1] · Takeo Furuya[1] · Akihiko Okawa[1] · Masaaki Aramomi[1] · Taigo Inada[1] · Koshiro Kamiya[1] · Mitsutoshi Ota[1] · Satoshi Maki[1] · Osamu Ikeda[1] · Kazuhisa Takahashi[1] · Chikato Mannoji[2] · Masashi Yamazaki[3]

Received: 4 August 2014 / Revised: 17 March 2015 / Accepted: 19 March 2015

Abstract
Purpose The motion at the non-ossified segment of the ossification of the posterior longitudinal ligament (OPLL) is thought to be highly correlated to aggravation of symptoms of myelopathy. The rationale for posterior decompression with instrumented fusion (PDF) surgery is to limit the motion of the non-ossified segment of OPLL by stabilization. The purpose of the present study was to elucidate the course of bone union and remodelling of the non-ossified segment of thoracic OPLL (T-OPLL) after PDF surgery.
Methods A total of 29 patients who underwent PDF surgery for T-OPLL were included in this study. We measured the thickness of the OPLLs by determining the thickest part of the OPLL in the sagittal multi-planer reconstruction CT images pre- and post-operatively. Five experienced spine surgeons independently performed CT measurements of OPLL thickness twice. Japanese Orthopaedic Association score for thoracic myelopathy was measured as clinical outcome measure.
Results Non-ossified segment of OPLLs fused in 24 out of 29 (82.8 %) patients. The average thickness of the OPLL at its thickest segment was 8.0 mm and decreased to 7.3 mm at final follow-up. The decrease in ossification thickness was significantly larger in the patients who showed fusion of non-ossified segments of OPLL compared with that in the patients did not show fusion. There was no significant correlation between the clinical outcome and the decrease in thickness of the OPLLs.
Conclusion The results of this study showed that remodelling of the OPLLs, following fusion of non-ossified segment of OPLLs, resulted in a decreased OPLL thickness, with potential for a reduction of spinal cord compression.

Keywords OPLL · Bone union · Fusion surgery · Remodelling

Introduction

In recent years, multi-slice computed tomography (CT) has exhibited added advantages for musculoskeletal imaging, including volumetric imaging and the ability to acquire multi-planar reconstructions (MPR). CT MPR images make it possible to obtain a precise observation of fine structures in an arbitrary plane that can be achieved following the acquisition of data from a single scan without the need for gantry angulation. Similarly, CT MPR images have been widely used to assess bony structures in the field of spinal surgery. By the acquisition of CT MPR sagittal images, the precise morphology of ossification of the posterior longitudinal ligament (OPLL) may be assessed, as opposed to via plain radiograms or conventional axial CT images, which have distinct limitations [1, 2]. CT MPR sagittal images of OPLL can reveal a non-ossified segment of the ossification at the thickest segment of ossification foci, even if the ossification seems to be continuous when classified by plain radiogram. The motion at the non-

✉ Masao Koda
masaokod@gmail.com

[1] Department of Orthopaedic Surgery, Chiba University Graduate School of Medicine, 1-8-1, Inohana, Chuo-Ku, Chiba 260-8670, Japan

[2] Department of Orthopaedic Surgery, Chiba Aoba Municipal Hospital, Chiba, Japan

[3] Department of Orthopaedic Surgery, University of Tsukuba, Tsukuba, Japan

Published online: 26 March 2015

ossified segment of the OPLL is thought to be highly correlated to aggravation of myelopathy [3]. Therefore, posterior decompression with instrumented fusion (PDF) has been indicated as one of the first-line treatment choice for patients with thoracic OPLL (T-OPLL), instead of posterior decompression alone [4]. The rationale for PDF surgery is to limit the motion of the non-ossified segment of OPLL by stabilization [5, 6].

Previous report revealed the bony fusion of non-ossified segment of OPLLs after PDF surgery. Following bony fusion, bone remodelling was also occasionally observed, which resulted in a reduction in the thickness of the ossification and an alteration from a sharp/angular morphology to one that was blunt [7].

The purpose of the present study was to elucidate the course of bone fusion and remodelling of the non-ossified segment of T-OPLL after PDF surgery.

Patients and methods

Study design

This was a retrospective cohort study.

Patient population

This study included patients who underwent PDF surgery for T-OPLL from September 2001 to May 2012 at our institute. A total of 29 patients (male 16 cases, female 13 cases) were included in this study. The average age of patients at the time of surgery was 53.4 years (range 22–74 years). The average number of fused segments was 8.1 (range 5–12 segments). The mean follow-up period was 68.8 months (range 17–147 months).

Surgical procedure

The patients underwent laminectomy at the spinal cord compression levels followed by posterior instrumented fusion with pedicle screw and rod system. The fused segments were two or three levels above and below the levels of laminectomy. Postero-lateral autologous bone graft was performed with local bone including resected spinous processes and laminae. We applied the posterior in situ fusion without correction of the spinal alignment.

CT image analysis

We assessed the non-ossified segment of OPLLs and measured the thickness of OPLLs at the thickest segment using pre-operative sagittal MPR images and post-operative follow-up CT scans. The CT images were acquired by continuous helical scanning (Aquilion 3; Toshiba Medical Systems, Tochigi, Japan) and sagittal plane reconstructed images were obtained (Vitrea software; Toshiba Medical Systems). Three consecutive sagittal images were acquired at 1 mm intervals, including a mid-sagittal slice; these were analysed for each patient.

Patients' OPLLs were classified into *linear*, *beaked*, *continuous waveform* and *continuous cylindrical* types by their morphology according to the previous reports [8, 9], but with a slight modification; we added the *circumscribed* type, identified when ossification was localised at the level of the disc without continuation between vertebrae (Fig. 1). Non-ossified segment of the ossification foci of the affected PLL was defined as the discontinuation of ossification as detected by CT reconstructed MPR images acquired in the sagittal plane. All patients in this series had non-ossified segment of ossification foci. We measured the thickness of the OPLLs by determining the thickest part of the OPLL in the three sagittal slices acquired during CT scanning. Five experienced spine surgeons independently performed CT measurements of OPLL thickness on 2 separate occasions of which interval was at least 3 days.

Clinical outcome measure

Our assessments were based on the Japanese Orthopaedic Association (JOA) score for cervical myelopathy, although we excluded the upper extremity motor and sensory functional scores as clinical outcome measures. The maximum JOA score is 11 points (Table 1).

We compared thoracic (T) JOA scores pre- and post-operatively, and the rate of recovery was computed by the following method: obtained points (i.e., post-operative JOA score – pre-operative JOA score)/pre-operative defect points (i.e., maximum score [11 points] – pre-operative JOA score) [10].

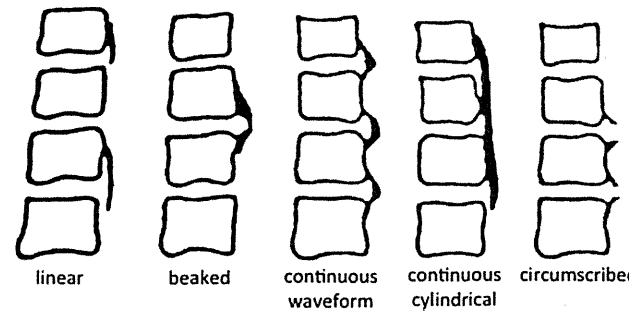

Fig. 1 The classification of thoracic OPLL by its morphology. Patients' OPLLs were classified into *linear*, *beaked*, *continuous waveform* and *continuous cylindrical* types by their morphology according to the previous reports, but with a slight modification; we added the *circumscribed* type, identified when ossification was localised at the level of the disc without continuation between vertebrae

Table 1 Japanese Orthopaedic Association score for thoracic myelopathy

Lower extremity motor function	
Unable to stand and walk by any means	0
Unable to walk without a cane or other support on a level	1
Capable of walk without support on a level but needs support on stairs	2
Capable of walk with clumsiness	3
Normal	4
Sensory function	
Trunk	
Apparent sensory disturbance	0
Minimal sensory disturbance	1
Normal	2
Lower extremity	
Apparent sensory disturbance	0
Minimal sensory disturbance	1
Normal	2
Bladder function	
Urinary retention or incontinence	0
Sense of retention or dribbling or thin stream or incomplete continence	1
Urinary retardation or pollakiuria	2
Normal	3

Statistical analysis

Inter-rater reliability and intra-rater reliability were expressed as R^2 value, both of which were assessed by expected mean square method and restricted maximum likelihood method, respectively. Inter-rater and intra-rater reliability determined with R^2 values were classified according to the previous report [11]: >0.81, almost perfect; 0.61–0.80, substantial; 0.41–0.60, moderate; 0.21–0.40, fair and 0–0.20, slight. Thickness of OPLL was compared between pre-operative and at final follow-up using paired t test. p value was determined as significant when it was smaller than 0.05. The correlation between the clinical outcome measure and the change in OPLL thickness was determined by Pearson's correlation coefficient test. The correlation between the follow-up period and the change in OPLL thickness was determined by Pearson's correlation coefficient test. All of the statistical analyses were performed with statistical software JMP version 10 (SAS Institute Japan, Tokyo, Japan).

Results

The morphology of the ossification was classified as follows: beaked type (5 cases), continuous waveform type (9 cases), continuous cylindrical type (12 cases) and circumscribed type (3 cases). Non-ossified segment of OPLLs fused in 24 out of 29 (82.8 %) patients over an average duration of 17.2 months (6–36 months) after the surgery. For 3 out of 5 (60 %) patients who exhibited no fusion of their non-ossified segment, the OPLL classification type was *circumscribed*.

Inter-rater reliability was calculated as substantial ($R^2 = 0.68$) and intra-rater reliability was calculated as moderate ($R^2 = 0.58$).

Preoperatively, the average thickness of the OPLL at its thickest segment was 8.0 mm (range 5.6–11.0 mm), decreased to 7.3 mm (range 5.3–9.0 mm) at final follow-up. The average decrease in thickness of OPLL was 0.8 mm (range 0.1–2.7 mm). There was significant difference between pre- and post-operative OPLL thickness (Fig. 1, $p = 0.004$; Fig. 2a–d). The average reduction of OPLL thickness in the patients who showed bony fusion of non-ossified segment was 1.2 mm (0.1–2.7 mm), whereas that in the patients who did not show bony fusion of non-ossified segment was 0.3 mm (0.1–0.5 mm). There was significant difference in reduction of OPLL thickness between the patients with and without bony fusion of non-ossified segment of OPLL ($p = 0.032$). There was no significant correlation between the clinical outcome and the decrease in thickness of the OPLLs. There was also no significant correlation between the follow-up period and the decrease in thickness of the OPLLs.

Discussion

The results of this study showed that remodelling of the OPLLs, following fusion of non-ossified segment of OPLLs, resulted in a decreased OPLL thickness, with potential for a reduction of spinal cord compression.

The precise mechanism underlying the reduction of OPLL thickness after PDF surgery is unclear. Our hypothesis is that the motion at the non-ossified segment stimulates the local thickening of the OPLL, therefore stabilization can reduce the ossification foci, of which mechanism might be similar to the reduction of protruded bony fragments in spinal canal of burst fracture cases after stabilization [12]. The other possible explanation is the pulsation of the thecal sac might reduce the size of ossification foci, of which mechanism is similar to the reduction of ossification of the ligamentum flavum after floating decompression procedure with instrumented fusion [13].

The present results may provide a possible rationale for PDF surgery to reduce the risk of the neurological deterioration by the motion at the residual anterior spinal cord compression by OPLL. In the past it was reported that neurological recovery after PDF surgery is gradual and peaks 9 months, on average, after surgery [14]. Our results

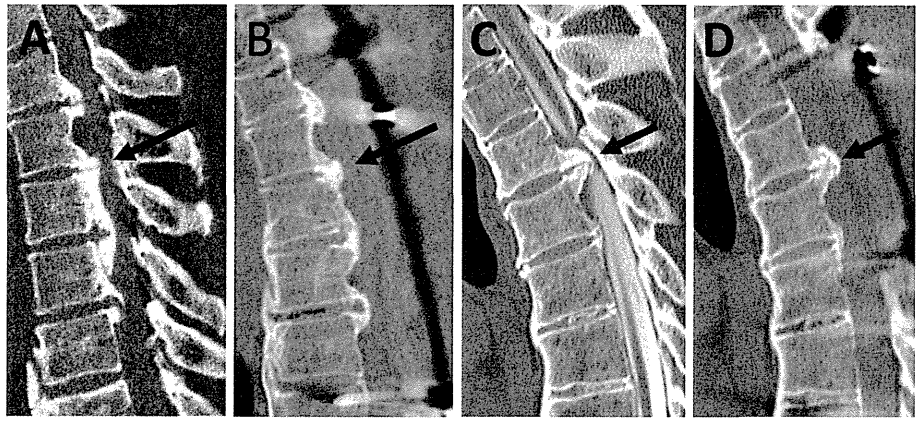

Fig. 2 Representative cases showing continuous waveform type OPLL (**a**, **b**) and beaked type OPLL (**c**, **d**). There was non-ossified segment at the thickest segment of OPLL (**a**, **c**; *arrows*). Several years after surgery, fusion of non-ossified segment and decrease in thickness of OPLL was observed (**b**, **d**; *arrows*)

showed that healing of non-ossified segment of OPLLs occurred 17 months, on average, after surgery. OPLL micro-motion after surgery may be a factor that slows neurological recovery.

The clinical significance of the bony fusion of a non-ossified segment of OPLL is still unclear. However, we speculate that motion occurring at a non-ossified segment of OPLL might contribute to repetitive minor damage to the spinal cord which could result in neurological deterioration. Thus, limiting motion in the compressed segment of the spinal cord is crucial for neurological recovery. According to the previous reports, neurological recovery achieved by PDF surgery was equivalent compared with the other surgical procedures, even though the spinal cord compression caused by the OPLL foci still remains after PDF surgery, suggesting that stabilization at the spinal cord compressed site is definitely important [5, 9, 12]. The present study revealed that bone union of the non-ossified segment of the ossification foci after PDF surgery, possibly providing additional stability to compressed spinal cord.

If remodelling is able to reduce the thickness of an OPLL, early fixation surgery can be beneficial for patients who show subclinical, or only mild myelopathy with a thickening OPLL and a disruption at the associated ossification foci. Future investigation is needed to clarify this point.

Conclusions

Non-ossified segment of OPLLs showed evidence of bony fusion, remodelling, and a decrease in thickness after PDF surgery for T-OPLL.

Conflict of interest None.

References

1. Smith ZA, Buchanan CC, Raphael D et al (2011) Ossification of the posterior longitudinal ligament: pathogenesis, management, and current surgical approaches. A review. Neurosurg Focus 30:E10
2. Kawaguchi Y, Matsumoto M, Iwasaki M et al (2014) New classification system for ossification of the posterior longitudinal ligament using CT images. J Orthop Sci 19:530–536
3. Fujiyoshi T, Yamazaki M, Okawa A et al (2010) Static versus dynamic factors for the development of myelopathy in patients with cervical ossification of the posterior longitudinal ligament. J Clin Neurosci 17:320–324
4. Matsumoto M, Chiba K, Toyama Y et al (2008) Surgical results and related factors for ossification of posterior longitudinal ligament of the thoracic spine: a multi-institutional retrospective study. Spine 33:1034–1041
5. Yamazaki M, Mochizuki M, Ikeda Y et al (2006) Clinical results of surgery for thoracic myelopathy caused by ossification of the posterior longitudinal ligament: operative indication of posterior decompression with instrumented fusion. Spine 31:1452–1460
6. Matsuyama Y, Sakai Y, Katayama Y et al (2009) Indirect posterior decompression with corrective fusion for ossification of the posterior longitudinal ligament of the thoracic spine: is it possible to predict the surgical results? Eur Spine J 18:943–948
7. Kimura H, Fujibayashi S, Takemoto M et al (2014) Spontaneous reduction in ossification of the posterior longitudinal ligament of the thoracic spine after posterior spinal fusion without decompression: a case report. Spine 39:E417–E419
8. Sakou T, Hirabayashi K (1994) Modified criteria of patient selection for treatment of ossification of spinal ligaments. Annual report of taskforce of research for ossification of spinal ligaments sponsored by the Japanese Ministry of Health and Welfare, pp 11–14 (in Japanese)
9. Matsumoto M, Toyama Y, Chikuda H et al (2011) Outcomes of fusion surgery for ossification of the posterior longitudinal ligament of the thoracic spine: a multicenter retrospective survey. J Neurosurg Spine 15:380–385
10. Hirabayashi K, Miyakawa J, Satomi K et al (1981) Operative results and postoperative progression of ossification among patients with ossification of cervical posterior longitudinal ligament. Spine 6:354–364
11. Kudo H, Yokoyama T, Tsushima E et al (2013) Interobserver and intraobserver reliability of the classification and diagnosis for

ossification of the posterior longitudinal ligament of the cervical spine. Eur Spine J 22:205–210
12. Sjöström L, Jacobsson O, Karlström G et al (1994) Spinal canal remodelling after stabilization of thoracolumbar burst fractures. Eur Spine J 3:312–317
13. Miyashita T, Ataka H, Tanno T (2013) Spontaneous reduction of a floated ossification of the ligamentum flavum after posterior thoracic decompression (floating method); report of a case (abridged translation of a primary publication). Spine J 13:e7–e9
14. Yamazaki M, Okawa A, Fujiyoshi T et al (2010) Posterior decompression with instrumented fusion for thoracic myelopathy caused by ossification of the posterior longitudinal ligament. Eur Spine J 19:691–698

Spine Publish Ahead of Print
DOI: 10.1097/BRS.0000000000001123

Reduced Field-of-View Diffusion Tensor Imaging of the Spinal Cord Shows Motor Dysfunction of the Lower Extremities in Patients with Cervical Compression Myelopathy

Satoshi Maki M.D.[1], Masao Koda M.D., PhD[1], Mitsutoshi Ota M.D.[1], Yoshihiro Oikawa M.D., PhD[1], Koshiro Kamiya M.D.[1], Taigo Inada M.D.[1], Takeo Furuya M.D., PhD[1], Kazuhisa Takahashi M.D., PhD[1], Yoshitada Masuda PhD[2], Koji Matsumoto[2], Masatoshi Kojima[2], Takayuki Obata M.D., PhD[3], Masashi Yamazaki M.D., PhD[4]

1. Department of Orthopaedic Surgery, Chiba University Graduate School of Medicine, Japan

2. Department of Radiology, Chiba University Hospital, Japan

3. Center for Charged Particle Therapy, National Institute of Radiological Sciences, Japan

4. Department of Orthopaedic Surgery, Faculty of Medicine, University of Tsukuba

Address correspondence and reprint requests to Satoshi Maki M.D., Department of Orthopaedic Surgery, Chiba University Graduate School of Medicine, 1-8-1 Inohana, Chuou-ku, Chiba 260-8670, Japan; E-mail: makisatoshi@hotmaill.com TEL: +8143-226-2117 FAX: +8143-226-2116

The manuscript submitted does not contain information about medical device(s)/drug(s). Initiative for Accelerating Regulatory Science in Innovative Drug, Medical Device, and Regenerative Medicine the Ministry of Health, Labour and Welfare, National Mutual Insurance Federation of Agricultural Cooperatives and The General Insurance Association of Japan grant funds supported this work. No relevant financial activities outside the submitted work.

Study Design. Cross-sectional study.

Objective. To quantify spinal cord dysfunction at the tract level in patients with cervical compressive myelopathy (CCM) using reduced field-of-view (rFOV) diffusion tensor imaging (DTI).

Summary of Background Data. Although magnetic resonance imaging (MRI) is the standard used for radiological evaluation of CCM, information acquired by MRI does not necessarily reflect the severity of spinal cord disorder. There is a growing interest in developing imaging methods to quantify spinal cord dysfunction. To acquire high-resolution DTI, a new scheme using rFOV has been proposed.

Methods. We enrolled 10 healthy volunteers and 20 patients with CCM in this study. The participants were studied using a 3.0 T MRI system. For DTI acquisitions, diffusion-weighted spin-echo rFOV single-shot echo-planar imaging was used. Regions-of-interest (ROI) for the lateral column (LC) and posterior column (PC) tracts were determined based on a map of fractional anisotropy (FA) of the spinal cord and FA values were measured. The FA of patients with CCM was compared with that of healthy controls and correlated with Japanese Orthopaedic Association (JOA) score.

Results. In LC and PC tracts, FA values in patients with CCM were significantly lower than in healthy volunteers. Total JOA scores correlated moderately with FA in LC and PC tracts. JOA subscores for motor dysfunction of the lower extremities correlated strongly with FA in LC and PC tracts.

Conclusions. It is feasible to evaluate the cervical spinal cord at the tract level using rFOV DTI. Although FA values at the maximum compression level were not well correlated with total JOA scores, they were strongly correlated with JOA subscores for motor dysfunction of the lower

extremities. Our findings suggest that FA reflects white matter dysfunction below the maximum compression level and FA can be used as an imaging biomarker of spinal cord dysfunction.

Key Words: diffusion tensor imaging; reduced field-of-view; magnetic resonance imaging; cervical spondylotic myelopathy; ossification of the posterior longitudinal ligament; fractional anisotropy; cervical disc herniation; atlantoaxial dislocation; spinal cord; corticospinal tract

Level of Evidence: 4

Mini Abstract

We evaluated functional disturbance in patients with cervical compressive myelopathy (CCM) using reduced field-of-view diffusion tensor imaging. Fractional anisotropy correlated strongly with gait disturbance in patients with CCM. Fractional anisotropy reflects white matter dysfunction and can be used as a biomarker of spinal cord dysfunction at the tract level.

Key Points

- It was feasible to evaluate the cervical spinal cord at the tract level using reduced field-of-view diffusion tensor imaging.
- Fractional anisotropy correlated strongly with gait disturbance in patients with cervical compressive myelopathy.
- Fractional anisotropy reflects white matter dysfunction below the level of maximum compression and can be used as an imaging biomarker of spinal cord dysfunction.

INTRODUCTION

Cervical compression myelopathy (CCM), including cervical spondylotic myelopathy, ossification of longitudinal ligament, and cervical disc herniation is a major cause of spinal cord disorder. Primarily, physical examination and imaging modalities including plain radiography, computed tomography (CT), and magnetic resonance imaging (MRI) are used to evaluate CCM clinically. MRI is the standard radiological evaluation of CCM, because it can reveal the degree of spinal cord compression and signal intensity changes in the spinal cord, neither of which can be obtained by plain radiographs or CT.[1–2] However, the information acquired by MRI does not necessarily reflect the severity of spinal cord disorder.[3] For example, it remains controversial whether there is significant correlation between intramedullary intensity changes obtained by T2-weighted MRI and severity of myelopathy symptoms. Therefore development of new imaging methods that can indicate the degree of spinal cord damage is under intense exploration.

Diffusion Tensor Imaging (DTI) can provide microstructural information about the spinal cord. Fractional anisotropy (FA) is derived from the diffusion matrix and represents the degree of anisotropy of a diffusion process. DTI has been used to evaluate patients with cervical spondylotic myelopathy.[4–12] DTI provides quantitative diffusion parameters. However, DTI has not been extensively used to evaluate specific spinal tract damage in patients with cervical spondylotic myelopathy because of the relatively lower spatial resolution limited by the achievable signal-to-noise ratio in previous studies.[4–8] A new method for reduced field-of-view (rFOV) has been proposed. The new rFOV diffusion method uses a spatially selective 2D echo-planar RF excitation pulse and a 180° refocusing pulse to reduce the FOV in the phase-encode direction, while simultaneously suppressing the signal from fat. This method allows the acquisition of high-resolution diffusion-weighted images and reduces susceptibility